Femtosecond Pump–Probe Analysis of Energy and Electron Transfer in Photosynthetic Membranes of *Rhodobacter capsulatus*†

Weizhong Xiao, Su Lin, Aileen K. W. Taguchi, and Neal W. Woodbury*

Department of Chemistry and Biochemistry and the Center for the Study of Early Events in Photosynthesis, Arizona State University, Tempe, Arizona 85287-1604

Received April 13, 1994®

ABSTRACT: Low-intensity, 295 K, femtosecond pump–probe transient absorption measurements are described that have been performed to investigate energy and electron transfer in photosynthetic membranes from a *Rhodobacter capsulatus* strain lacking functional light harvesting antenna complex II. Spectral and kinetic similarities between the absorption changes of isolated reaction centers and those of reaction centers in membranes upon 800-nm excitation suggest that the charge separation process in both cases is very similar. An ultrafast energy relaxation process observed near 872 nm when 800-nm excitation is used is interpreted as interexcitonic relaxation within the antenna, though other interpretations, such as vibrational relaxation, are possible. On the basis of global exponential fitting analysis of the time-dependent spectral changes using 800- and 880-nm excitation wavelengths to selectively excite the reaction center and the LHI antenna, respectively, it is found that excitation energy transfer and trapping in *Rb. capsulatus* is limited by the overall rate of energy transfer between the antenna and the reaction center. This conclusion is supported by the observation that excitation at 800 nm, but not 880 nm, results in absorbance changes indicative of charge separation with a lifetime (3.1 ps) very close to that reported for charge separation in isolated reaction centers (3.5 ps). Thus, most reaction centers that are directly excited undergo charge separation and not backward energy transfer to the LHI antenna complexes. Both a kinetic model analysis and a direct comparison between time-resolved spectra obtained using different excitation wavelengths resulted in an energy-detrapping efficiency of about 15 ± 10%.

The initial solar energy conversion reactions of photosynthesis involve absorption of light by membrane-bound antenna complexes followed by transfer of the energy to a reaction center complex, where charge separation takes place. Purple photosynthetic bacteria are among the best characterized organisms in the study of the molecular mechanisms of energy and electron transfer, due to the availability of the X-ray crystal structures of reaction centers isolated from *Rhodopseudomonas* (*Rp.*)[1] *viridis* (Deisenhofer et al., 1984) and *Rhodobacter* (*Rb.*) *sphaeroides* (Allen et al., 1987; Chang et al., 1991) and to the fact that the organization of the photosynthetic apparatus in purple bacteria is somewhat simpler than that in most other photosynthetic organisms (Zuber, 1985; Hawthornthwaite & Cogdell, 1991).

The organization of the photosynthetic apparatus in purple nonsulfur bacterial membranes has been studied extensively using both biochemical and spectroscopic methods [for a review, see Hawthornthwaite and Cogdell (1991)]. In wild type (wt) *Rb. capsulatus*, there are two types of light-harvesting complexes, B880 (or light harvesting complex I, LHI) and B800–850 (or light harvesting complex II, LHII), named after their Q_y absorption maxima. Several other purple bacteria are found to contain only B880 antenna complexes, such as *Rhodospirillum* (*Rs.*) *rubrum*. In species containing multiple types of antenna complexes, it has sometimes been possible to construct or select mutants which lack functional B800–850 antenna complexes (Youvan et al., 1985; Hunter et al., 1989), leaving only the B880 and reaction center complexes.

Electron microscopy has suggested that LHI and the reaction center form a closely-associated core complex with the reaction center located in the center (Stark et al., 1984). Biochemical analysis has also shown that this core complex contains about 30 Bchls per reaction center in a fixed stoichiometry for a variety of species and growth conditions (Thornber et al., 1983). It is generally accepted that the basic building block for the LHI complex is a heterodimer of two polypeptides, α and β, that binds a Bchl dimer (Cogdell et al., 1982; Gimenénez-Gallergo et al., 1986). Despite the apparent uniformity of the $\alpha\beta$ subunit building blocks of the anetenna, the LHI spectrum is thought to be heterogeneously broadened to a small extent (Reddy et al., 1993; Kramer et al., 1984), indicating the existence of several different environments of the antenna chromophores. It has been suggested that low-energy spectral forms of the LHI antenna may help to concentrate the excitations prior to their transfer to the reaction center (van Grondelle et al., 1987).

Charge separation in isolated wild type reaction centers has been characterized in detail using a variety of absorption and emission experiments with high time resolution [for reviews, see Kirmaier and Holten (1987, 1993), Parson (1991), and Woodbury and Allen (1994)]. The present understanding of photosynthetic electron transfer is that charge separation occurs with a time constant of about 3.5 ps, from the excited

† This work was supported by Grants DMB91-58251 and MCB-9219378 from the National Science Foundation. Instrumentation was purchased with funds from NSF Grant DIR-8804992 and Department of Energy Grants DE-FG-05-88-ER75443 and DE-FG-05-87-ER75361. This is publication No. 202 from Arizona State University Center for the Study of Early Events in Photosynthesis. The Center is funded by DOE Grant DE-FG-88-ER13969 as a part of the USDA/DOE/NSF Plant Science Centers Program.

* To whom correspondence should be addressed.

® Abstract published in *Advance ACS Abstracts,* June 15, 1994.

[1] Abbreviations: *Rb.*, *Rhodobacter*; *Rp.*, *Rhodopseudomonas*; *Rs.*, *Rhodospirillum*; PMS, phenazine methosulfate; wt, wild type; LHI, light harvesting complex I; LHII, light harvesting complex II; P, bacteriochlorophyll dimer; Bchl or B, bacteriochlorophyll; Bphe or H, bacteriopheophytin; Q, quinone; ps, picosecond; fs, femtosecond; EDTA, ethylenediaminetetraacetic acid.

0006-2960/94/0433-8313$04.50/0

singlet state of the primary electron donor (P*) to $Bphe_A$, the bacteriopheophytin acceptor associated with the active branch of the reaction center, forming the state $P^+Bphe_A^-$. P is a dimer of bacteriochlorophyll (Bchl) molecules. This initial charge separation process is followed by a subsequent electron-transfer reaction from $Bphe_A$ to Q_A (a ubiquinone) with an overall time constant of about 200 ps. Recently, Schmidt et al. (1993) found that the primary photosynthetic reactions in whole membranes of a *Rb. capsulatus* mutant lacking both LHI and LHII are very similar to those in isolated reaction centers.

Study of the charge separation kinetics of the reaction center in the presence of light-harvesting complexes has been much more difficult. This is due in part to the extensive spectral overlap between antenna and reaction center pigment absorption bands making it difficult to either selectively excite or selectively probe reaction center optical transitions. In addition, very low excitation intensity must be used to avoid singlet–singlet annihilation, a process known to quench the excited singlet state of the antenna and alter the early-time kinetics of excitation quenching (Bakker et al., 1983). Because of these technical difficulties, direct measurements of P* decay and $P^+Bphe_A^-$ formation upon selective excitation of the reaction center have not been made with subpicosecond time resolution. This is an important measurement, however, since it provides a direct answer to the question, is energy trapping in the antenna limited by the rate of charge separation in the reaction center?

Two extreme kinetic models have been considered to describe energy transfer in the antenna and trapping by the reaction center. The trap-limited model (Pearlstein, 1982; Borisov, 1990) assumes that charge separation is the rate-limiting step in excitation trapping. This implies that the excitation visits the reaction center forming P* many times before charge separation occurs. The other extreme case is the diffusion-limited model or migration-limited model (Fetisova et al., 1985), which assumes that the energy-trapping rate is limited by the rate of energy transfer from the antenna to the reaction center. In this model the initial charge separation in the reaction center is much faster than the overall backward energy transfer to the antenna. Once an excitation reaches the reaction center, charge separation essentially always occurs. Several studies have indicated that the dynamics of energy transfer and trapping in purple photosynthetic bacteria is trap-limited. For example, using model calculations based on picosecond time-resolved fluorescence measurements, Müller et al. (1993) concluded that, at room temperature, the energy-trapping kinetics in the entire antenna system of wild type *Rb. capsulatus* is limited by the reaction center charge separation. However, other studies have favored an excitation migration limited model. Measurements of the fluorescence excitation spectrum of photosynthetic membranes indicate that, for various purple bacterial species, there is essentially no contribution of the reaction center bands to the excitation spectra of antenna fluorescence (Otte et al., 1993). These results suggest that the energy-detrapping efficiency is very low in most of the purple photosynthetic bacteria. The detrapping efficiency here is defined as the percentage of the total number of excitations reaching the reaction center that transfer back to the antenna.

An attempt to determine the detrapping efficiency from time-resolved spectroscopy has also been made recently (Timpmann et al., 1993). By exciting the chromatophores from *Rs. rubrum* with a 15–20-ps pulse in the 800-nm band of the reaction center and probing the antenna bleaching or fluorescence, 25% and 40% of the excitation energy was found to be transferred back to the antenna for photochemically fully active (PBHQ) and prereduced ($PBHQ^-$) reaction centers, respectively. These estimates of the detrapping efficiency assumed equal absorption coefficients at 800 nm for the B880 antenna and the reaction center. These absorption coefficients are critical to the value obtained for detrapping efficiency and are difficult to measure accurately. In addition, it was necessary to assume that the backward energy transfer from the photochemically inactive or closed reaction center (P^+BHQ) to the antenna is completely blocked, an assumption which again is difficult to verify experimentally. These assumptions could be avoided by performing faster time-resolution transient absorption measurements and directly observing the initial charge separation event upon selective excitation of the reaction center.

Recently, several studies have been performed on ultrafast energy transfer in antenna complexes (Reddy et al., 1992, 1993; Hess et al., 1993). Hole-burning spectra of membranes from *Rb. sphaeroides* (Reddy et al., 1992) indicated that LHI is largely homogeneously broadened, and this has been interpreted as a consequence of exciton level structure and ultrafast interexciton level scattering. However, no subpicosecond resolution spectroscopic studies have been performed on such processes in LHI-containing membranes, and thus there is little direct information about the kinetics of the ultrafast evolution of the LHI antenna excited state in its natural form.

In the present work, we describe a detailed study of energy and electron transfer in membranes of an LHII-depleted *Rb. capsulatus* mutant using femtosecond time-resolved pump–probe transient absorption spectroscopy. Low-intensity excitation at either 880 or 800 nm was utilized to allow comparison of the trapping kinetics due to selective excitation of either the antenna or the reaction center. Electron-transfer kinetic measurements on isolated reaction centers have also been performed using excitation at 800 nm.

MATERIALS AND METHODS

Bacterial Strains. The construction and characterization of the *Rb. capsulatus* strain used for these studies has been reported elsewhere (Taguchi et al., 1993). Briefly, the plasmid, pCR (Taguchi et al., 1993) containing the α and β genes of LHI as well as the L and M genes of the reaction center, derived from pU2922 (Youvan et al., 1985; Bylina et al., 1986), was transformed into *Escherichia coli* S17-1 (Simon et al., 1983) and conjugated into U43, a deletion strain of *Rb. capsulatus* lacking most of the *puf* operon and containing a point mutation which eliminates the LHII Bchl pigments from the photosynthetic membrane (Youvan et al., 1985).

Bacterial Growth, Chromatophore Preparation, and Reaction Center Preparation. Cells were grown microaerobically in the dark in a rich medium, RCVPY, which contains 0.1% $(NH_4)_2SO_4$, 0.4% DL-malic acid, 9.6 mM potassium phosphate buffer (pH 6.8), 0.2% Difco yeast extract, 0.2% peptone, and 5% super salts (for 1 L, 0.4 g of disodium EDTA, 4 g of $MgSO_4 \cdot 7H_2O$, 1.5 g of $CaCl_2 \cdot 2H_2O$, 20 mL of trace elements, 0.24 g of $FeSO_4 \cdot 7H_2O$, 20 mg of thiamine). For 250 mL of trace elements, the following ingredients were added: 0.4 g of $MnSO_4 \cdot H_2O$, 0.7 g of H_3BO_3, 0.01 g of $Cu(NO_3)_2 \cdot 3H_2O$, 0.06 g of $ZnSO_4 \cdot 7H_2O$, and 0.19 g of $Na_2MoO_4 \cdot 2H_2O$. The cells were harvested by low-speed centrifugation, resuspended in a minimal amount of 10 mM phosphate buffer (pH 7.35), and disrupted by passage through a French pressure cell once at 20 000 psi. The cell debris was removed by centrifugation

at 8000 rpm for 15 min in a Sorvall GS-3 rotor. The supernatant was then recentrifuged at 45 000 rpm for 2.5 h in a Beckman 45 Ti rotor. The resultant pellet, which contains mainly the ruptured, resealed photosynthetic membranes (chromatophores), was resuspended in 50 mM phosphate buffer (pH 7.35), homogenized in a glass tissue grinder, and stored at −20 °C as a stock for future use. All measurements were performed at room temperature. For the transient absorption measurements, the membrane stock was diluted with 50 mM phosphate buffer (pH 7.35) to an optical density of 1.3 at 875 nm in a spinning cell with an optical path length of 2.5 mm and a diameter of 18 cm. To facilitate rereduction of the reaction center initial electron donor, PMS and ascorbic acid were added to a final concentration of 50 μM and 25 mM, respectively. For some measurements, isolated reaction centers were extracted from the chromatophores and purified as described previously (Taguchi et al., 1992).

Femtosecond Pump–Probe Absorption Spectroscopy. The femtosecond pump–probe absorption apparatus has been described in detail previously (Taguchi et al., 1992). For this work, roughly 200 μJ, 590-nm, 150-fs pulses emerging from a three-stage dye amplifier were split into two equal parts and used as excitation and probe beams. The excitation beam was passed through a flowing water cell to generate a white-light continuum. Continuum pulses were sent through either an 800- or an 880-nm (depending on the excitation wavelength) interference filter with a spectral bandwidth of 10 nm and were then reamplified in a prism amplifier (Santa Ana Laser) pumped with about 2 mJ of 532-nm light from a 540-Hz regenerative amplifier (Continuum). The beam was attenuated with neutral density filters to achieve the desired excitation intensities and then focused on the sample. The dyes used for continuum amplification at 800 and 880 nm were LDS799 and LDS890, respectively. The probe beam was first sent through a variable time-delay stage before continuum generation. After continuum generation, the probe pulse was further split into two equal parts, as sample and reference beams. The sample beam was passed through the excited region of the sample while the reference beam was passed through an unexcited region. The two beams were then focused into two separate optical fibers which were coupled to a monochromator (Acton Research Corporation Model Spectra Pro 275). The spectra were acquired on a dual diode array optical multichannel analyzer (Princeton Instruments Models DPAA-1024 and ST121) at 0.14 nm/channel and were averaged over 10^4 laser shots at each time delay. The relative polarization of the pump and probe beams was set at the magic angle.

The spinning sample cell was rotated at 2 revolutions/second (sample velocity of 500 cm/s) so that the excited region of the sample was removed in the 2-ms interval between excitation pulses. The excitation beam intensity was attenuated with neutral density filters before being focused on the sample. The final excitation intensity was adjusted so that for each excitation pulse fewer than 20% of reaction centers were excited (Lin et al., 1994). This corresponds to a pulse energy of about 2 μJ/pulse focused on a 2-mm spot.

Kinetic data were analyzed using global exponential decay analysis as described previously (Taguchi et al., 1992). In general, the experimental data, $\Delta A(\lambda_{probe},t)$, were fitted to a sum of exponentials,

$$\Delta A(\lambda_{probe},t) = \sum_{i=1}^{n} A_i(\lambda_{probe}) \exp(-t/\tau_i)$$

where τ_i's are lifetimes of kinetic components, λ_{probe} is the wavelength of the probing light, and $A_i(\lambda_{probe})$'s are the preexponential amplitude spectra or decay-associated spectra. A locally written nonlinear least squares minimization algorithm was used in the fitting procedure, and the goodness of the fit was judged by comparing the χ^2 error for fits with different numbers of exponential terms and by assessing the randomness of the distribution of the fitting residuals.

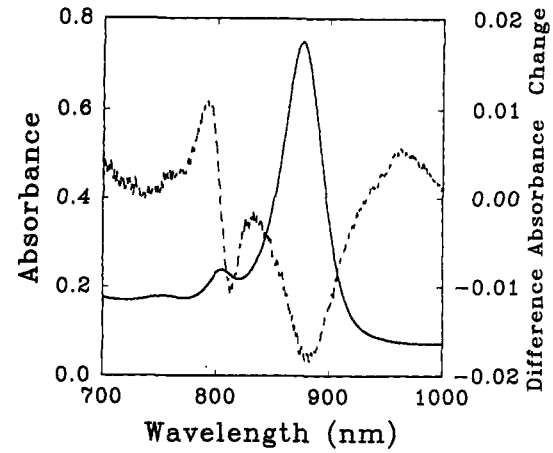

FIGURE 1: Room temperature ground-state absorbance (solid line) and light-minus-dark (dashed line) difference absorbance spectra of chromatophores from the LHII-deficient strain of *Rb. capsulatus* in the near-IR region. Spectra were taken on a Varian Cary-5 spectrometer modified to accept the input of an actinic light source via a fiber optic cable. The maximum absorbance change is only 20% of the total change with saturating actinic light, and the light bleaching is reversible.

RESULTS

Ground-State Absorption Spectrum. Figure 1 shows the room temperature absorption spectrum of chromatophores from the LHII$^-$ strain of *Rb. capsulatus* used in these studies. The absorption bands at 760 and 800 nm are predominantly due to Bphes and monomer Bchls in the reaction center, respectively. The 880-nm band is mainly due to the Q_y transition of the LHI antenna (or B880), though there is a small contribution from the reaction center primary electron donor as well. A significant amount of absorption in the 760–800-nm region also comes from the blue tail of the B880 antenna absorption band. Since U43, the *Rb. capsulatus* strain used, lacks functional LHII and the associated transitions at 800 and 850 nm, the spectrum shown is very similar to that of *Rs. rubrum* membranes (Hawthornthwaite & Cogdell, 1991) or isolated core complexes from various purple photosynthetic bacteria (Hawthornthwaite & Cogdell, 1991; Thornber et al., 1983), both of which contain just the LHI antenna and the reaction centers. Also shown in Figure 1 is the light-minus-dark difference absorption spectrum of the chromatophores. The broad bleaching centering around 878 nm is presumably due to bleaching of the Q_y transition of ground-state P in the reaction center. The first derivative type spectral shape around 800 nm, indicative of formation of the charge-separated state P^+HQ^-, presumably corresponds to an electrochromic shift of the reaction center monomer Bchls due to P^+ formation.

Femtosecond Pump–Probe Measurements with 800-nm Excitation. Energy- and electron-transfer kinetics were first studied by exciting the chromatophores at 880 nm with a 10-nm-wide (full width at half-maximum) 150-fs pulse. At this wavelength more than 95% of the light is absorbed by LHI antenna Bchls (estimated from the magnitude of the spectral features in Figure 1 and the known absorption

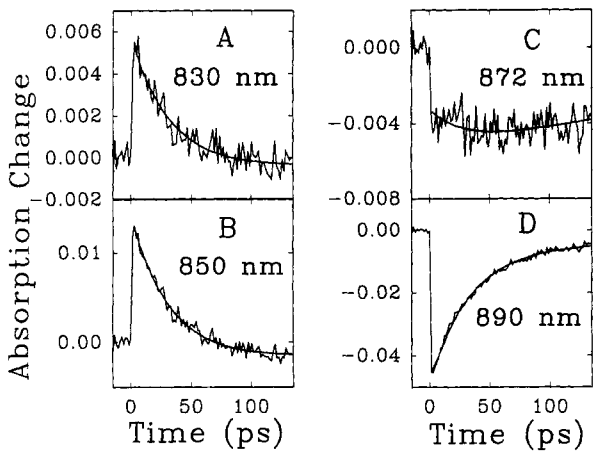

FIGURE 2: Time-resolved absorption changes at four probing wavelengths, (A) 830 nm, (B) 850 nm, (C) 872 nm, and (D) 890 nm, upon exciting chromatophores with 880-nm light. Spectra were taken at 1.5-ps intervals over a 150-ps time scale.

spectrum of isolated reaction centers). Transient absorption difference spectra were measured every 1.5 ps over a 150-ps time range in the spectral region between 754 and 904 nm. Global analysis of the time vs wavelength absorbance change surface was performed as described in Materials and Methods. The analysis was performed separately in the 754–820-nm region, where the reaction center charge separation dominates the absorption changes, and in the 830–904-nm region, where the absorbance changes are dominated by the formation and decay of the LHI excited singlet state. The decay profiles at four selected wavelengths in the 830–904-nm region are shown in Figure 2. They are similar to the transient absorption decay spectra obtained for *Rs. rubrum* with a time resolution of ≈10 ps (Sundström et al., 1986). On the shorter wavelength side of the 830–904-nm region (below 868 nm), an apparent absorption increase at zero time due to B880* (Nuys et al., 1985) is observed. This absorption increase decays with a time constant of about 36 ps to a long-lived weak bleaching. On the longer wavelength side (above 868 nm), an instantaneous absorption decrease is observed upon excitation. This initial bleaching also recovers with biexponential kinetics, involving a 36-ps component and a slowly decaying component. The complete preexponential amplitude spectra in the 830–904-nm region obtained from a global analysis using two exponential components $[A_1(\lambda)\exp(-k_1t) + A_2(\lambda)\exp(-k_2t)$, as described in Materials and Methods] are presented in Figure 3A. Introducing an additional exponential decay component did not significantly improve the value of χ^2 or the shape of the fitting residuals. The 36-ps component dominates the decay kinetics throughout the region. The negative amplitude associated with the 36-ps component peaks around 890 nm, about 10 nm red-shifted from the center of the ground-state antenna absorption band. The other kinetic component obtained (magnified in the inset of Figure 3A) has a lifetime of about 330 ps. This lifetime is longer than the time scale of the measurement and thus probably represents a mixture of long-lived components (see Discussion). It displays negative amplitude throughout the spectral region analyzed and is maximal near 880 nm.

Absorption changes associated with the formation of the charge-separated state of the reaction center dominate the spectral region between 754 and 820 nm. The results from the global exponential decay analysis of this region are shown in Figure 3B. The fitting again yielded two components, one with a lifetime of 36 ps and the other a constant on the time scale of the measurement. The absorbance changes on the

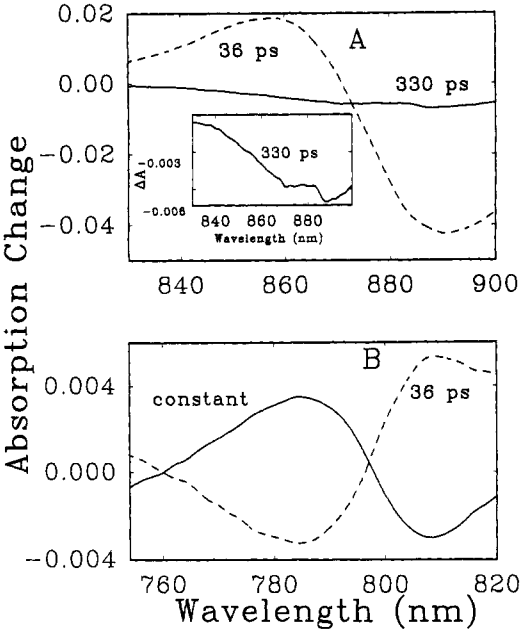

FIGURE 3: Amplitude spectra resulting from a global exponential decay analysis of time vs wavelength absorption change surfaces collected for chromatophores in the spectral regions (A) 830–904 nm and (B) 754–820 nm on a 150-ps time scale, using 880-nm excitation. The times shown are the time constants associated with each amplitude spectrum. The inset in panel A shows a 10-fold expansion of the 330-ps component.

36-ps time scale correspond to formation of the charge-separated state ($P^+Bphe_A^-$) in the reaction center from excited antenna. The amplitude spectrum of the constant term corresponds to the slow decay of the resultant $P^+Bphe_A^-$ state. The spectrum of $P^+Bphe_A^-$ obtained is similar to that found in isolated reaction centers (Kirmaier & Holten, 1988).

Femtosecond Pump–Probe Measurements with 800-nm Excitation. In order to determine the detrapping efficiency and to observe the direct forward charge separation in the reaction center (i.e., $P^* \rightarrow P^+Bphe_A^-$), transient absorption difference spectra using 800-nm excitation were recorded. At this excitation wavelength, the blue side of the Q_y transition of the antenna and the 800-nm band of the reaction center were simultaneously excited (Figure 1).

Figure 4A,B shows the global analysis of transient absorption changes recorded every 2.5 ps over 250 ps and every 0.15 ps over 15 ps at 2-nm intervals in the spectral region between 830 and 904 nm. In general, the time constants and amplitude spectra resulting from the fits on both time scales resemble those shown above for 880-nm excitation; the kinetics are again dominated by the 36–39-ps decay component, which displays negative amplitude on the longer wavelength side and positive amplitude on the shorter wavelength side of the 830–904-nm region. This indicates that, in this spectral region, the same kinetic processes are dominant using either 880- or 800-nm excitation. The kinetics in the 15-ps scan can be well approximated by a single exponential past the first 700 fs, characterized by only the 36–38-ps decay constant (Figure 4B). This is because, in a 15-ps scan, it is not possible to resolve the 36-ps component and the lower amplitude slow phase. For the same reason, the size of the positive amplitude of this component near 855 nm relative to that of the negative amplitude near 890 nm is reduced on the 15-ps time scale due to the fact that the negative amplitude of the long-lived (constant) term partially cancels the positive amplitude of the 36-ps decay component.

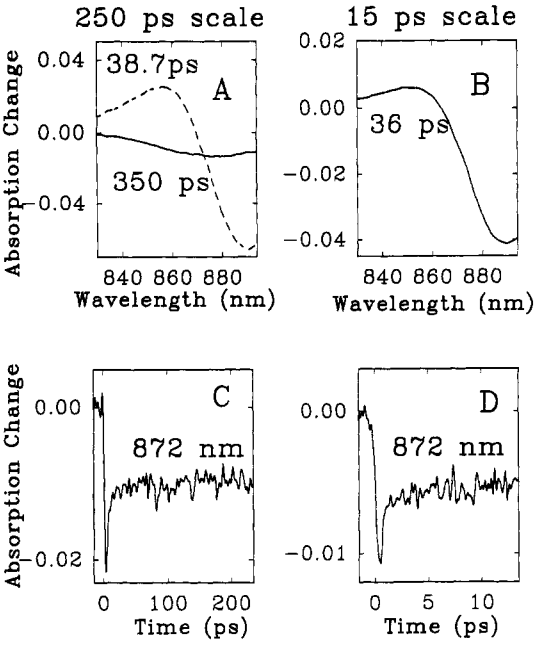

FIGURE 4: Amplitude spectra obtained from a global exponential decay analysis of the time vs wavelength absorption change surfaces of chromatophores in the spectral region between 830 and 904 nm over (A) a 250-ps time range and (B) a 15-ps time range, using 800-nm excitation. Spectra were obtained at 2.5- and 0.15-ps intervals for the 250- and 15-ps time ranges, respectively. Kinetic traces probing at 872 nm are shown for (C) the 250-ps scan and (D) the 15-ps scan.

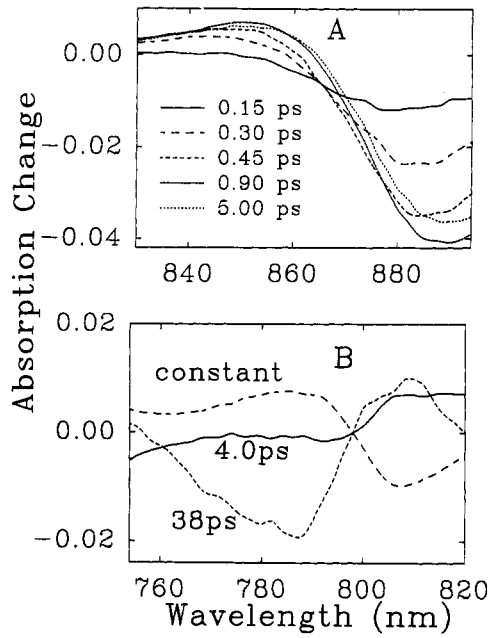

FIGURE 5: (A) Time-resolved absorption change spectra of chromatophores in the 830–904-nm region, with excitation at 800 nm. (B) Amplitude spectra of chromatophores resulting from a global exponential decay analysis of time-resolved absorption change spectra in the 754–820-nm region taken every 2.5 ps using 800-nm excitation. The time constants associated with each amplitude spectrum are shown.

Despite the overall similarity, there are several significant differences between the measurements performed at the two excitation wavelengths. First, the initial absorption decrease shifts rapidly from 880 to 890 nm when the sample is excited by the 800-nm light (Figure 5A), an effect not observed with 880-nm excitation (data not shown). This spectral shift is complete within 900 fs. This fast kinetic process is also clearly evident in the kinetic curves around 872 nm, where very little

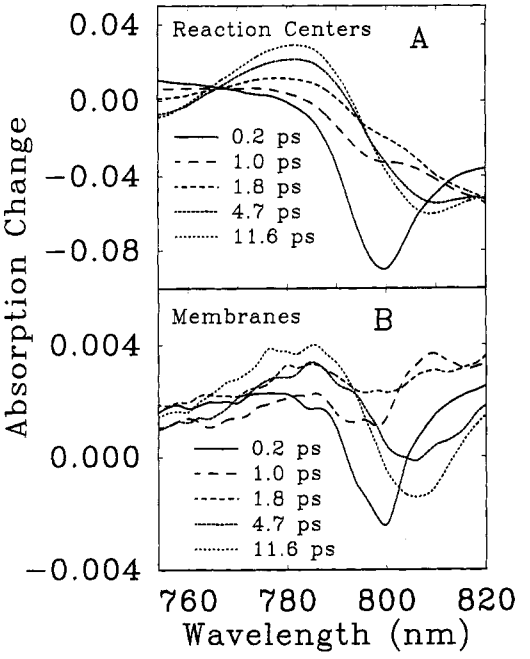

FIGURE 6: Time-resolved absorption change spectra at various times after 800-nm excitation, probing between 754 and 820 nm, obtained for (A) isolated reaction centers and (B) chromatophores.

absorption change is observed during the transition between the excited state at 1 ps and the long-lived charge-separated state (Figure 4C,D). It should be noted here that this ultrafast process has been excluded from the global analysis described above by fitting the data from 700 fs onward. The possible origins of this fast decay phase shall be discussed below.

A second difference between 800-nm excitation and 880-nm excitation can be seen in the spectral shape and the time constant (350 ps) of the slow kinetic component shown in Figure 4A. Though the kinetic and spectral properties of this component when 800-nm excitation is used are similar to those when 880-nm excitation is used (Figure 3A), a slightly larger amplitude for this component is observed with 800-nm excitation relative to the amplitude of the 36–39-ps component.

Transient absorption change spectra in the region between 754 and 820 nm were also obtained on both 15- and 250-ps time scales using 800-nm excitation. Figure 5B presents the results of a global exponential decay analysis for the 250-ps scan. Two exponential decay terms and a constant are required to adequately describe the kinetics in this spectral region. Besides the 36–38-ps component and the constant term, an additional 4-ps component was observed. Since the 4-ps component is too fast to be accurately characterized on the 250-ps time scale, data were also collected and analyzed on a 15-ps time scale. Figure 6B shows the absorption change spectra at several delay times. For comparison, also shown in Figure 6A are the spectra obtained on the same time scale for isolated reaction centers from *Rb. capsulatus*, following excitation with an 800-nm flash. In both cases, an absorption decrease near 800 nm developed instantaneously upon excitation, reaching a maximum at 200 fs (the approximate duration of the excitation pulse), and decayed completely at 1 ps, when the electrochromic shift due to charge separation started to grow in.

The data collected in the spectral region between 754 and 820 nm on the 15-ps time scale were analyzed by global exponential decay analysis. Panels A and B of Figure 7 show the amplitude spectra and time constants obtained for isolated reaction centers and membranes, respectively. In both cases,

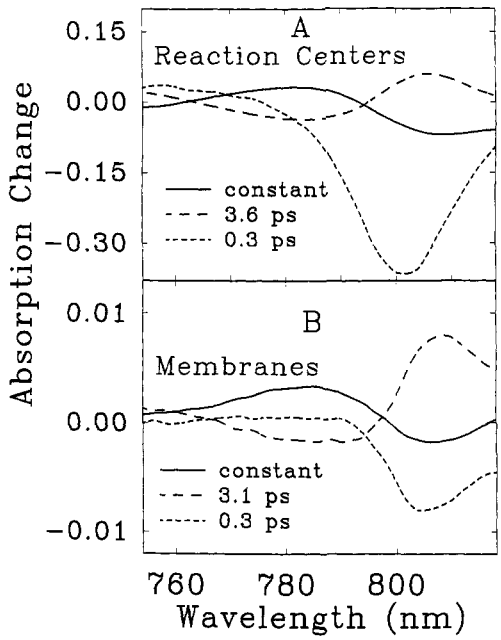

FIGURE 7: Amplitude spectra obtained from a global exponential decay analysis of the time vs wavelength absorption change surfaces of (A) isolated reaction centers and (B) chromatophores in the spectral region between 754 and 820 nm on a 15-ps time scale, using 800-nm excitation. The time constants associated with each amplitude spectrum are shown. The amplitude spectrum of the constant component in panel B, which essentially represents the amount of charge-separated state formed via direct forward charge separation from P*, is used to estimate the detrapping efficiency.

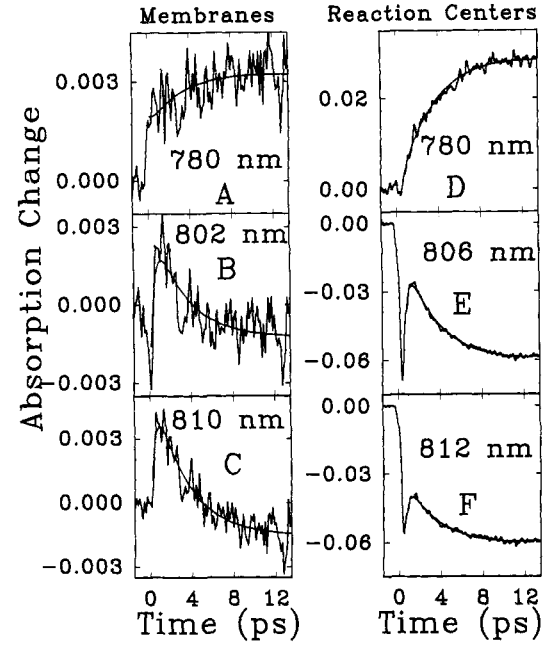

FIGURE 8: The kinetics of absorption changes at several representative probe wavelengths on the 15 ps timescale for both chromatophores (A: 780 nm, B: 802 nm and C: 810 nm) and isolated reaction centers (D: 780 nm, E: 806 nm and F: 812 nm), using 800 nm excitation.

the data could be described by two exponential decay components and a constant. The fastest component, with a lifetime of about 300 fs, in both isolated reaction centers and chromatophores, represents the ultrafast kinetic event described above (similar results have been obtained previously in isolated reaction centers; Breton et al., 1986). The 3.6-ps component in the isolated reaction center represents the formation of the charge-separated state from the excited state, and the lifetime is consistent with values obtained using other excitation wavelengths (Kirmaier & Holten, 1988). The 3.1-ps component observed in chromatophores has both a time constant and an amplitude spectrum which are similar to those of the 3.6-ps component in isolated reaction centers. It should be noted here that the 15-ps scan is too short to resolve the 38-ps component (obtained previously in the 250-ps scan with 800-nm excitation) from the slow decay of the $P^+Bphe_A^-$ state (lifetime $\approx$ 200–250 ps in isolated reaction centers) (Kirmaier & Holten, 1987). In fact, all the time scales used in the present work are not long enough to resolve a 250-ps component accurately, especially considering the small amplitude of the absorbance changes associated with charge separation in chromatophores. To show the goodness of the curve fitting and the similarity between the absorption changes in chromatophores and isolated reaction centers, fits of time traces at three selected wavelengths from the global analysis are presented in Figure 8. The fitting starts from 200 fs onward.

DISCUSSION

Femtosecond transient absorption spectroscopy utilizing low-intensity tunable infrared pulses was used to investigate the time-dependent spectral changes in photosynthetic membranes of an LHII$^-$ strain of *Rb. capsulatus*. In the following sections, energy transfer and trapping in whole chromatophores will be discussed and compared to the electron-transfer kinetics in isolated reaction centers. Then, two independent methods will be used to determine the energy-detrapping efficiency.

Ultrafast Relaxation Processes in LHI. Hole-burning measurements of antenna complexes in membranes from *Rb. sphaeroides* (Reddy et al., 1993) have suggested that B875 (B880 for *Rb. capsulatus*) is largely homogeneously broadened ($\Gamma_H \approx 200$ cm^{-1}), which has been interpreted as a result of exciton level structure and ultrafast interexciton level scattering. Spectral hole burning on the red edge of the B880 antenna band showed that, at 4.2 K, the homogeneous width of the B896 zero-phonon hole is about 3.2 cm^{-1}, corresponding to a total optical dephasing time of 6.6 ps. A favored interpretation is that the B896 band, previously thought to be a spectrally distinct entity (Hunter et al., 1989), is due to the lowest exciton energy level of the B880* and the 6.6-ps dephasing is due to exciton scattering with energetically inequivalent neighboring unit cells (Reddy et al., 1993). Picosecond relaxation processes have also been detected by previous time-resolved fluorescence spectroscopy studies [reviewed by Valkunas et al. (1991)]. The time traces around 872 nm with excitation at 800 nm (Figure 4C,D) provide additional evidence for subpicosecond energy relaxation process in the chromatophores of *Rb. capsulatus*. In the time-resolved spectra (Figure 5A), this process corresponds to a rapid early-time spectral red shift. As is in the case of hole burning, the ultrafast energy relaxation process may arise from a downhill interexcitonic level relaxation. The absence of the ultrafast process in the transient absorption spectra with 880-nm excitation is consistent with this hypothesis since 880 nm is close to the lowest exciton band ($\approx$896 nm) of B880* (Reddy et al., 1993). The reason that the 6.6-ps dephasing present in the hole-burning spectra of B896 was not observed in the transient absorption spectra with either 800- or 880-nm excitation may be that the exciton scattering with energetically inequivalent neighboring unit cells causes little absorption change on this time scale at room temperature. The process of interexcitonic level relaxation could manifest itself in a time-dependent shift in the absorption change spectra

when the higher exciton bands near 800 nm are excited directly and energy in this transition is transferred to lower lying transitions on the subpicosecond time scale. Two other alternatives, vibrational relaxation and inhomogeneity, have been previously considered to interpret the ultrafast decay processes in antenna complexes (Hess et al., 1993). Hole-burning spectra show that a weakly coupled 750-cm^{-1} vibrational mode, with $S = 0.05$, dominates the B875 band (Reddy & Small, 1991). With such a small Franck–Condon factor and so high a vibrational frequency, one would not expect to significantly populate higher level vibronic states and, therefore, vibrational relaxation should not be a major contributor to the ultrafast energy decay process. Since the inhomogeneous broadening for B880 ($\Gamma_I = 80$ cm^{-1}) (Reddy et al., 1993) is much smaller than the homogeneous broadening, we speculate that inhomogeneity should not be responsible for this ultrafast decay process either, though this explanation has been suggested by others (Pullerits & Freiberg, 1990) and cannot be ruled out on the basis of the data reported here.

The ultrafast transient (lifetime $\approx$ 300 fs) near 800 nm, present in isolated reaction centers using 800-nm excitation (Figures 6A and 7A), has also been observed previously and has been interpreted as a short-lived excited state of the monomer Bchls (Breton et al., 1986). This ultrafast component is also evident in whole membranes when 800-nm excitation is used (Figures 6B and 7B), showing the similarities between the photochemistry of membrane-bound and isolated reaction centers.

Energy Trapping in LHI. The lifetime (37 ± 3 ps) for the major decay of the B880 excited state obtained in this work with the reaction center in an active (open) state is very similar to the value (≈40 ps) obtained previously in low excitation intensity picosecond time-resolved fluorescence measurements on the same chromatophores (Woodbury & Bittersmann, 1990). This implies that both low-intensity transient absorption and time-resolved fluorescence record the same excitation decay process and indicate that the amount of singlet–singlet annihilation in the present study is minimal. The effect of annihilation was also investigated by varying the intensity of the excitation pulse. A 2-fold increase in the excitation intensity did not appreciably alter the trapping kinetics. The lack of a dependence of the kinetics on intensity indicates that annihilation processes were not dramatically affecting the observed kinetics. This fact is somewhat surprising, given the results of some previous annihilation studies (Valkunas et al., 1991) which indicated that kinetic manifestations of annihilation were significant at excitation levels lower than those used in this study (see Materials and Methods). This is probably the result of the fact that in *Rb. capsulatus* the LHI/RC core complexes normally communicate through LHII antenna complexes. In this mutant, which lacks functional LHII, communication between LHI complexes may be greatly impaired.

The spectral shape of the 36-ps component (Figures 4A,B and 5A) and the kinetic traces in the 830–904-nm region (Figure 2), in general, follow the spectral characteristics of B880* of *Rs. rubrum* obtained by Sundström et al. (1986). The fact that the center of the antenna bleaching is around 890 nm, about 10 nm red-shifted from the ground state Q_y absorption peak of B880, is presumably due to a significant contribution from stimulated emission of B880*. This is consistent with the spontaneous emission spectrum which centers around 895 nm (Woodbury & Bittersmann, 1990). The instantaneous absorption increase below 870 nm (Figure 2) is probably due to absorption by B880*. This instantaneous absorption increase is also seen in the amplitude spectrum of the 36-ps component (Figure 3A). It should be noted that the positive/negative feature of the 36-ps component amplitude spectrum in Figure 3A may also partially reflect the energy-transfer process from the antenna to the reaction center, forming P*, though this is probably a small effect.

Two spectrally overlapping components may contribute simultaneously to the amplitude spectrum of the slowly decaying component in the 830–904-nm region when 880-nm excitation is used (Figure 3A). A similar amplitude spectrum is also observed for the long-lived component upon 800-nm excitation (Figure 4A). While the spectral amplitude in the shorter wavelength region (<880 nm) is probably due primarily to long-lived charge-separated states ($P^+H_A^-Q_A$ and/or $P^+H_AQ_A^-$), the bleaching at longer wavelengths (>880 nm) probably represents thermal repopulation of B880*. This interpretation is consistent with the observation that 5–10% of the fluorescence from B880* decays on the 200-ps time scale (Woodbury & Bittersmann, 1990), corresponding to the kinetics of electron transfer from $Bphe_A$ to Q_A. This slowly decaying fluorescence is thought to be back electron transfer re-forming B880* from $P^+H_A^-Q_A$. It is likely that the excited-state absorption of the slowly decaying B880* (which has a broad positive amplitude in the 855-nm region, Figure 5A), to some extent, cancels the negative amplitude of the P^+ absorption change around 875 nm. Although the two slow processes should decay on different time scales (P^+ lives for milliseconds while thermal repopulation of B880* should decay with $P^+H_A^-Q_A$ on the 200-ps time scale), they were not easily resolved due to their small amplitudes and the limited time scale used in these experiments. An attempt was made to resolve the slow varying B880* decay by performing the global exponential decay analysis on the data taken on the 250-ps time scale using 800-nm excitation in the narrow spectral region between 880 and 904 nm, in which the absorbance changes should be dominated by the thermal repopulation of B880*. Two components (lifetimes = 36 and 247 ps) resulted from this fit with an amplitude ratio between the fast and the slow components of about 20:1 (not shown). These results are in good agreement with what has been observed by time-resolved fluorescence experiments (Woodbury & Bittersmann, 1990). In addition, the two components have similar pre-exponential amplitude spectra, consistent with the hypothesis that both components arise from a single species, i.e., B880*.

The observation that the absorption decrease due to bleaching of the Q_y transition of ground state P (≈875 nm) in the membrane (Figures 3A and 4A) is shifted by roughly 25 nm to the red from that observed in the isolated reaction center (Kirmaier & Holten, 1988) is in accord with the steady-state light-minus-dark difference spectrum (Figure 1). Considering that the Stokes shift of the LHI antenna complex (≈190 cm^{-1}) is much smaller than that of the reaction center (≈835 cm^{-1}) [based on known absorption and emission spectra of isolated reaction centers (Woodbury & Allen, 1994) and the B880 antenna (Woodbury & Bittersmann, 1990)], it seems likely that, in membranes of *Rb. capsulatus*, the zero–zero transition energy of P is below that of B880. This suggests that forward energy transfer from B880* to P* is energetically favorable. A similar spectral red shift of the zero–zero transition of the special pair in other purple photosynthetic membranes has also been reported previously by Kleinherinbrink et al. (1992).

Extinction Coefficient of LHI Absorption Changes. One of the most striking aspects of the evolution of the absorption changes during the energy-trapping process is the large loss

of oscillator strength between the initial excited state of the antenna at early times and the charge-separated state which remains on long time scales. This can be seen in the kinetic traces of Figure 2C,D where the reaction center is expected to have significant absorption changes in the charge-separated state at long times due to the bleaching of the Q_y band of P; yet this long-lived absorbance change is an order of magnitude smaller than that due to bleaching of the Q_y band of B880 and stimulated emission from B880* at early times. A similar conclusion can be drawn from Figure 3A, where the amplitude spectrum of the 330-ps component (which has a large contribution from the charge-separated state) is much smaller than the sum of the 36- and 330-ps component amplitude spectra which should represent the absorbance difference spectrum of the initial excited state [see, for example, Woodbury and Allen (1994)]. Since this discrepancy cannot be attributed to annihilation (see above), one must conclude that the extinction coefficient of the absorbance decrease near 880 nm associated with the LHI excited state for a single excitation is nearly an order of magnitude larger than that due to bleaching of the Q_y band of P. Part of this discrepancy results from the fact that B880* shows both a bleaching of the Q_y band of the antenna and stimulated emission while P^+ formation results only in bleaching of the Q_y band of P, but this accounts for only about half of the discrepancy. This large difference in extinction coefficients is odd, since both B880 and P are thought to be made up of a dimer of Bchl molecules. This has been noted previously (Novoderezhkin & Razjivin, 1993) and has been taken as evidence for a strong exciton coupling between Bchl pairs in LHI. This is consistent with the idea of ultrafast interexciton relaxation in the LHI antenna described above.

Charge Separation in Membranes. In isolated reaction centers, charge separation kinetics can be measured by monitoring either the decay of stimulated emission from P* or the formation of charge-separated states. In LHI-containing membranes, however, the stimulated emission from P* is masked by large absorption changes from the antenna and the electron-transfer kinetics can only be clearly detected around 800 nm where reaction center transitions are comparable to or larger than those from the antenna. As in isolated reaction centers, the formation of charge-separated states in membranes induces an electrochromic shift in the Q_y transition energy of the monomer Bchls (Figure 1), as is manifested by a first-derivative-type absorption change spectrum near 800 nm (Kirmaier & Holten, 1987).

When 880-nm excitation is used, charge separation occurs with a single exponential lifetime of 36 ps (Figure 3). This is because at this wavelength the initial excited state is almost exclusively B880*, and the rate of charge separation is determined by the overall migration and trapping process. The biphasic kinetics of charge separation observed using excitation at 800 nm (Figures 5B and 7B) is due to the simultaneous excitation of the antenna and the reaction center at this wavelength. The slow component (38 ps) presumably has the same origin as that observed in the case of 880-nm excitation, corresponding to the formation of the charge-separated state after energy transfer from B880* to P*. The observation of a fast kinetic phase resulting in absorbance changes indicative of charge separation with a lifetime very close to that for charge separation in isolated reaction centers (Figure 7) provides compelling evidence that most direct excitation of P undergoes charge separation and not energy transfer to LHI (see below for a quantitative treatment).

The similarities between the transient spectra around 800 nm of the membrane and the isolated reaction center (Figures 3B, 5B, 6, and 7) suggest that charge separation in membranes and isolated reaction centers is similar. This observation is in agreement with results obtained by Schmidt et al. (1993) on membrane-bound reaction centers of a *Rb. capsulatus* strain which lacks both LHI and LHII, though the charge separation rate in the antennaless membranes is $(4.5\ \text{ps})^{-1}$ in comparison to $(3.6\ \text{ps})^{-1}$ in isolated reaction centers (Figure 7A). It is not clear whether $(4.5\ \text{ps})^{-1}$ is the true electron-transfer rate of reaction centers in LHI-containing membranes or whether complete elimination of the antenna, particularly LHI, in photosynthetic membranes perturbs the structure of the reaction center and therefore alters the electron-transfer rate.

Intrinsic Energy-Transfer Rates and Energy-Detrapping Efficiency. In order to obtain the intrinsic energy-transfer rates and to determine the energy-detrapping efficiency, the following kinetic scheme is proposed:

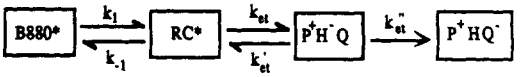

(1)

where k_1 represents the rate of energy transfer from the antenna to the reaction center (RC), k_{-1} represents the total energy detrapping rate, k_{et} and k_{et}' are the forward and the backward electron-transfer rates, respectively, and k_{et}'' is the secondary electron-transfer rate. If one assumes that k_{et}' and k_{et}'' are much smaller than k_{et}, three approximate eigenvalues can been obtained:

$$\lambda_1 = \frac{(k_1 + k_{-1} + k_{et}) + [(k_1 + k_{-1} + k_{et})^2 - 4k_1k_{et}]^{1/2}}{2} \quad (2)$$

$$\lambda_2 = \frac{(k_1 + k_{-1} + k_{et}) - [(k_1 + k_{-1} + k_{et})^2 - 4k_1k_{et}]^{1/2}}{2} \quad (3)$$

$$\lambda_3 = k_{et}'' + \frac{k_{et}'k_{-1}}{k_{et} + k_{-1}} \quad (4)$$

From eqs 2 and 3, the following relationships can also be established:

$$\lambda_1\lambda_2 = k_1k_{et} \quad (5)$$

$$\lambda_1 + \lambda_2 = k_1 + k_{-1} + k_{et} \quad (6)$$

Here λ_1^{-1}, λ_2^{-1}, and λ_3^{-1} correspond to the three experimental time constants 3.1 ± 0.1 ps, 37 ± 2 ps, and 247 ± 30 ps, respectively. The latter time constant was determined by analyzing the decay of the long-lived LHI excited state due to thermal repopulation from $P^+Bphe_A^-$ (see above). For each species, the amplitude corresponding to each component depends on the initial excitation condition. From the above kinetic scheme, one would expect that the lifetime of the fast charge separation component in the membrane (λ_1^{-1}) should be shorter than its counterpart in isolated reaction centers. This is because λ_1 is largely determined by the sum of the competitive rates, k_{et} (charge separation) and k_{-1} (energy transfer from P* to B880*). Substituting the values of λ_1 and λ_2 and the assumed value for k_{et} of 3.6 ps as determined in isolated reaction centers (Figure 7A) into eqs 5 and 6, one obtains $k_1 = (31.9 \pm 0.4\ \text{ps})^{-1}$ and $k_{-1} = (25.0 \pm 6.0\ \text{ps})^{-1}$. It should be noted here that the error in k_{-1} is significantly larger than that in k_1 due to the fact that k_{et} and λ_1 are much larger than k_1 and λ_2 (see eq 6). On the basis of the above

analysis, an approximate energy-detrapping efficiency (defined as $k_{-1}/(k_{et} + k_{-1})$ or, equivalently, as the percentage of excitation energy on P* that transfers back to the antenna) of 13 ± 3% is obtained (the error is calculated from the fitting error associated with λ_1 and λ_2). In addition, from eq 4, it can be seen that the lifetime of the third component (λ_3) is mainly determined by the secondary electron-transfer rate (k_{et}'') because k_{et} is much larger than k_{-1} and, therefore, the second term in eq 4 is probably small.

Obviously, the above calculation of the detrapping efficiency assumed that the rate of electron transfer from P* to $P^+Bphe_A^-$ in intact antenna-reaction complexes was the same as that in isolated reaction centers. If a slower time constant for electron transfer were assumed, a larger detrapping efficiency would be calculated. For example, a value for k_{et} of $(4.5\ ps)^{-1}$ [as reported by Schmidt et al. (1993)] would result in a detrapping efficiency of 28% [$k_1 = (25.4\ ps)^{-1}$, $k_{-1} = (11.4\ ps)^{-1}$]. In either case, the kinetic model suggests that most of the time when P* is formed, charge separation occurs, supporting the concept that it is the rate of energy transfer between A* and P* that limits the overall rate of energy trapping in the membrane.

A second approach to estimating the detrapping efficiency is to use spectral information to quantify the amounts of intermediate states at different times in the energy-trapping process. This procedure relies on the ability to differentiate the P^+ formation which results from direct excitation of LHI from that which results from direct excitation of the reaction center. This can be done approximately by assuming that, in the Q_y region of the spectrum, the observed absorption changes immediately after excitation are almost entirely due to the excited state of LHI. Making this assumption allows one to estimate the amount of B880* formed under the two excitation conditions. This assumption follows from the argument, made above, that in this region of the spectrum, absorption changes due to B880* are roughly an order of magnitude larger than absorption changes due to P*, for an equivalent population of the two states. [The argument made above was phrased in terms of P^+, but it should hold as well in terms of P*, since the magnitude of the absorption changes for the two states in this region are known to be almost the same from studies of isolated reaction centers (Kirmaier & Holten, 1988).] Thus, for the calculations which follow, the assumption is made that regardless of whether 800- or 880-nm excitation is used, the absorption change at 904 nm represents predominantly the population of the state B880*. It is also assumed that the quantum yields of energy trapping and charge separation are excitation wavelength independent.

By comparing the absorption change at 904 nm immediately (0.75 ps) after excitation with 880-nm light to the amount of P^+ formed at long times (100 ps) under the same excitation conditions, one can determine the amount of P^+ which results from a set amount of B880*. One can then estimate the amount of B880* formed directly upon 800-nm excitation by looking at the absorption change at 904 nm and then calculate the amount of P^+ which should result from this B880*, based on the results of the 880-nm-excitation experiment. In practice, this amounts to normalizing the absorption changes using 880-nm excitation to those using 800-nm excitation at 0.75 ps and 904 nm and then subtracting the spectra observed at long times (100 ps) in the 790–820-nm region using 880-nm excitation from that using 800-nm excitation. The results of such a calculation are shown in Figure 9. The solid line is the total absorption change due to P^+ at 100 ps after exciting with 800-nm light (P^+_{total}). The short dashed line shows the

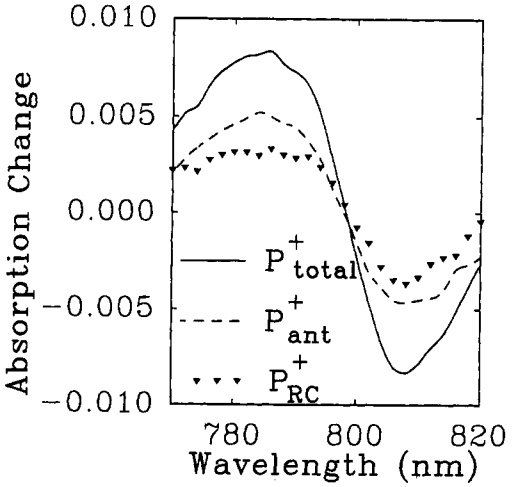

FIGURE 9: P^+ absorbance difference spectra in the 770–820-nm region obtained from a spectral analysis of the time-dependent absorption changes in chromatophores using 800-nm excitation. P^+_{total} is the total P^+ difference spectrum after 100 ps. P^+_{ant} is the difference spectrum of the P^+ due to direct excitation of the antenna, and P^+_{RC} is the difference spectrum of P^+ due to direct excitation of the reaction center.

amount of the total P^+ absorption change which results from direct excitation of B880 with the 800-nm-excitation light (P^+_{ant}).

The remaining P^+ formed at long time should be that which results from direct excitation of the reaction center at 800 nm. This is called P^+_{RC} in Figure 9. One can see that the amount of P^+ formation due to direct excitation of the reaction center at 800 nm is characterized by a difference absorption change between 786 and 807 nm of about 0.006. This can then be compared to the amount of P^+ formed immediately upon charge separation after 800-nm excitation. This is shown in Figure 7B. The amplitude spectrum of the constant term in this figure gives the spectrum of the $P^+Bphe_A^-$ formed with a 3.1-ps time constant (recall that the data collection time after excitation in this experiment was only 12 ps and, therefore, the 37-ps absorption changes are not resolved). The difference absorption change on this time scale between 786 and 807 nm is about 0.005. Thus, 85 ± 10% of the P* formed directly by 800-nm excitation results in charge separation with a 3.1-ps time constant. Therefore, 15 ± 10% of the direct excitation of P* results in detrapping. This agrees well with the estimates made above solely on the basis of kinetic model analysis.

In conclusion, the experimental data presented in this work imply that the spectral and kinetic parameters of absorbance changes associated with charge separation in isolated reaction centers and membranes are very similar. In addition, the ultrafast energy relaxation of the excited antenna around 872 nm observed using 800-nm excitation probably arises from interexcitonic relaxation in LHI, though other relaxation processes in the excited state, such as vibrational relaxation, cannot be ruled out on the basis of this data alone. Finally, both kinetic model analysis and comparison of time-resolved spectra from excitation at 800 and 880 nm resulted in an energy-detrapping efficiency of 15 ± 10% from the excited singlet state of the reaction center primary electron donor to the B880 antenna, with the precise value depending on the analysis methods employed and the assumptions used. This implies that the rate-limiting step in energy trapping in membrane-bound LHI–reaction center complexes is the transfer of excitation from LHI to the reaction center.

ACKNOWLEDGMENT

The authors would like to thank Drs. S. H. Lin, R. Blankenship, M. Hayashi, F. Kleinherenbrink, A. Freiberg, and Mr. J. M. Peloquin for helpful discussions and for providing preprints of important publications.

REFERENCES

Allen, J. P., Feher, G., Yeates, T. O., Komiya, H., & Rees, D. C. (1987) *Proc. Natl. Acad. Sci. U.S.A. 84*, 5730–5734.

Bakker, J. G. C., van Grodelle, R., & Den Hollander, W. Th. F. (1983) *Biochim. Biophys. Acta 725*, 508–518.

Borisov, A. Y. (1990) *Photosynth. Res. 23*, 283–289.

Breton, J., Martin, J.-L., Petrich, J., Migus, A., & Antonetti, A. (1986) *FEBS Lett. 9*, 37–43.

Bylina, E. J., Ismail, S., & Youvan, D. C. (1986) *Plasmid 16*, 175–181.

Chang, C.-H., El-Kabbani, O., Tiede, D., Norris, J., & Schiffer, M. (1991) *Biochemistry 30*, 5352–5360.

Cogdell, R. J., Linsay, J. G., Valentine, J., & Durant, I. (1982) *FEBS Lett. 150*, 151–154.

Deisenhofer, J., Epp., O., Miki, K., Huber, R., & Michel, H. (1984) *J. Mol. Biol. 180*, 385–398.

Fetisova, Z. G., Borisov, A. Y., & Fok, M. V. (1985) *J. Theor. Biol. 112*, 41–75.

Gimenénez-Gallergo, G., Fenoll, C., & Ramiréz, J. M. (1986) *Anal. Biochem. 152*, 29–34.

Hawthornthwaite, A. M., & Cogdell, R. J. (1991) in *Chlorophylls* (Scheer, H., Ed.) pp 493–528, CRC Press, Boca Raton.

Hess, S., Feldchtein, F., Babin, A., Nurgaleev, I., Pullerits, T., Sergeev, A., & Sundström, V. (1993) *Chem. Phys. Lett. 216*, 247–257.

Hunter, C. N., van Grondelle, R., & van Dorssen, R. J. (1989) *Biochim. Biophys. Acta 973*, 383–389.

Kirmaier, C., & Holten, D. (1987) *Photosynth. Res. 13*, 225–260.

Kirmaier, C., & Holten, D. (1988) *Isr. J. Chem. 28*, 79–85.

Kirmaier, C., & Holten, D. (1993) in *The Photosynthetic Reaction Center* (Deisenhofer, J., & Norris, J. R., Eds.) Vol. II, pp 49–70, Academic Press, San Diego.

Kleinherenbrink, F. A. M., Deinum, G., Otte, S. C. M., Hoff, A. J., & Amesz, J. (1992) *Biochim. Biophys. Acta 1099*, 175–181.

Kramer, H. J. M., Pennoyer, J. D., van Grondelle, R., Westerhuis, W. H. J., Niederman, R. A., & Amesz, J. (1984) *Biochim. Biophys. Acta 767*, 335–344.

Lin, S., Chiou, H.-C., Kleinherenbrink, F. A. M., & Blankenship, R. E. (1994) *Biophys. J. 66*, 437–445.

Müller, M. G., Drews, G., & Holzwarth, A. R. (1993) *Biochim. Biophys. Acta 1142*, 49–58.

Novoderezhkin, V. I., & Razjivin, A. P. (1993) *FEBS Lett. 330* (1), 5–7.

Nuys, A. M., van Grondelle, R., Joppe, H. L. P., Van Bochove, A. C., & Duysens, L. N. M. (1985) *Biochim. Biophys. Acta 810*, 94–105.

Otte, S. C. M., Kleinherenbrink, F. A. M., & Amesz, J. (1993) *Biochim. Biophys. Acta 1143*, 84–90.

Parson, W. W. (1991) in *Chlorophylls* (Scheer, H., Ed.) pp 1153–1180, CRC Press, Boca Raton.

Pearlstein, R. M. (1982) in *Photosynthesis, Energy Conversion By Plants and Bacteria* (Govindjee, Ed.) Vol. 1, pp 293–329, Academic Press, New York.

Pullerits, T., & Freiberg, A. (1990) *Chem. Phys. 149*, 409–418.

Reddy, N. R. S., & Small, G. J. (1991) *J. Chem. Phys. 94* (11), 7545–7546.

Reddy, N. R. S., Picorel, R., & Small, G. J. (1992) *J. Phys. Chem. 96*, 6458–6464.

Reddy, N. R. S., Cogdell, R. J., & Small, G. J. (1993) *Photochem. Photobiol. 57* (1), 35–39.

Schmidt, S., Arlt, T., Hamm, P., Lauterwasser, C., Finkele, U., Drews, G., & Zinth, W. (1993) *Biochim. Biophys. Acta 1144*, 385–390.

Simon, R., Priefer, U., & Puhler, A. (1983) *Bio/Technology 1*, 784–791.

Stark, W., Kühlbrandt, K., Wildhaber, I., Wehri, E., & Mühlethaler, K. (1984) *EMBO 3*, 777–783.

Sundström, V., van Grondelle, R., Bergström, H., Åkesson, E., & Gillbro, T. (1986) *Biochim. Biophys. Acta 851*, 431–446.

Taguchi, A. K. W., Stocker, J. W., Alden, R. G., Causgrove, T. P., Peloquin, J. M., Boxer, S. G., & Woodbury, N. W. (1992) *Biochemistry 31*, 10345–10355.

Taguchi, A. K. W., Stocker, J. W., Boxer, S. G., & Woodbury, N. W. (1993) *Photosynth. Res. 36*, 43–58.

Thornber, J. P., Cogdell, R. J., Pierson, B. K., & Seftor, R. E. B. (1983) *J. Cell. Biochem. 23*, 159–169.

Timpmann, K., Zhang, F. G., Freiberg, A., & Sundström, V. (1993) *Biochim. Biophys. Acta 1183*, 185–193.

Valkunas, L., Liuolia, V., Freiberg, A. (1991) *Photosynth. Res. 27*, 83–95.

van Grondelle, R., Bergström, H., Sundström, V., & Gillbro, T. (1987) *Biochim. Biophys. Acta 894*, 313–326.

Woodbury, N. W., & Allen, J. P. (1994) in *Anoxgenic Photosynthetic Bacteria* (Blankenship, R. E., Madigan, M. T., & Bauer, C. E., Eds.) Advances in Photosynthesis, Kluwer Academic Publishers, Dordrecht, Netherlands (in press).

Woodbury, N. W., & Bittersmann, E. (1990) in *Current Research in Photosynthesis*, Vol. II, pp 165–168, Kluwer Academic Publishers, Dordrecht, Netherlands.

Youvan, D. C., Ismail, S., & Bylina, E. J. (1985) *Gene 38*, 19–30.

Zuber, H. (1985) *Photochem. Photobiol. 42*, 821–844.